

Magnetic excitations in two-leg spin 1/2 ladders: experiment and theory

M. Grüninger,¹ M. Windt,¹ T. Nunner,² C. Knetter,³ K.P. Schmidt,³ G.S. Uhrig,³ T. Kopp,² A. Freimuth,¹
U. Ammerahl,^{1,5} B. Büchner,^{1,4} and A. Revcolevschi⁵

¹*II. Physikalisches Institut, Universität zu Köln, 50937 Köln, Germany*

²*Experimentalphysik VI, Universität Augsburg, 86135 Augsburg, Germany*

³*Institut für Theoretische Physik, Universität zu Köln, 50937 Köln, Germany*

⁴*II. Physikalisches Institut, RWTH-Aachen, 52056 Aachen, Germany*

⁵*Laboratoire de Chimie des Solides, Université Paris-Sud, 91405 Orsay Cédex, France*
(September 26, 2001)

Magnetic excitations in two-leg $S=1/2$ ladders are studied both experimentally and theoretically. Experimentally, we report on the reflectivity, the transmission and the optical conductivity $\sigma(\omega)$ of undoped $\text{La}_x\text{Ca}_{14-x}\text{Cu}_{24}\text{O}_{41}$ for $x=4, 5$, and 5.2 . Using two different theoretical approaches (Jordan-Wigner fermions and perturbation theory), we calculate the dispersion of the elementary triplets, the optical conductivity and the momentum-resolved spectral density of two-triplet excitations for $0.2 \leq J_{\parallel}/J_{\perp} \leq 1.2$. We discuss phonon-assisted two-triplet absorption, the existence of two-triplet bound states, the two-triplet continuum, and the size of the exchange parameters.

I. Introduction

Low-dimensional quantum antiferromagnets offer a diverse view on quantum fluctuations at work. Particular interest has focused on two-leg spin 1/2 ladders, which show a spin liquid ground state with a spin gap to the lowest excited state, and superconductivity under pressure upon hole doping [1]. In undoped two-leg ladders the existence of two-“magnon” (two-triplet) bound states was predicted theoretically by a number of groups [2–7]. Recently, we have reported on the observation of a two-triplet bound state with $S_{\text{tot}}=0$ in the optical conductivity spectrum of $(\text{La,Ca})_{14}\text{Cu}_{24}\text{O}_{41}$ [9], a compound with stacked layers of Cu_2O_3 ladders and of CuO_2 chains. Concerning the peak positions and the line shape of the bound states, good agreement was achieved between experiment and two different theoretical approaches, namely, Jordan-Wigner fermions and perturbation expansion using unitary transformations [9]. Using the second approach, some of us have discussed the momentum-resolved spectral densities and the relationship between fractional (spinons) and integer excitations (triplets) in two-leg spin 1/2 ladders [10]. In these proceedings, we discuss recent experimental and theoretical progress that we have achieved.

II. Experiment

Single crystals of $\text{La}_x\text{Ca}_{14-x}\text{Cu}_{24}\text{O}_{41}$ were grown by the travelling solvent floating zone method [11]. These so called telephone number compounds have attracted particular interest due to the possibility of hole doping. Here, we are interested in the magnetic properties of nominally undoped samples, i.e. Cu^{2+} , which corresponds to $x=6$. Single phase crystals could only be synthesized for $x \leq 5.2$ [11]. The samples studied here with $x=5.2, 5$, and 4 on average contain $n=0.8/24, 1/24$ and

$2/24$ holes per Cu, respectively. However, x-ray absorption data show that for these low doping levels the holes are located within the chains [12]. Thus, we consider the ladders to be undoped [9].

In order to determine the optical conductivity $\sigma(\omega)$ we have measured both transmission and reflection data between 500 and 12000 cm^{-1} on a Fourier spectrometer. The transmittance $T(\omega)$ and the reflectivity $R(\omega)$ were calibrated against a reference aperture and a gold mirror, respectively. The optical conductivity $\sigma(\omega) = n\kappa\omega/2\pi$ was determined by inverting [13,14]

$$R(\omega) = [(n-1)^2 + \kappa^2] / [(n+1)^2 + \kappa^2], \quad (1)$$

$$T(\omega) = [(1-R)^2\Phi] / [1-(R\Phi)^2], \quad (2)$$

$$\Phi(\omega) = \exp(-2\omega\kappa d/c) = \exp(-\alpha d), \quad (3)$$

where n denotes the index of refraction, κ the extinction coefficient, α the absorption coefficient, c the velocity of light and d the thickness of the transmission sample [$R(\omega)$ denotes the single bounce reflectivity and hence needs to be measured on a thick (“semi-infinite”), opaque sample]. Equation 2 is obtained for a sample with parallel surfaces by adding up the intensities of all multiply reflected beams *incoherently*, i.e., by neglecting interference effects. Experimentally, this condition is realized either if the sample surfaces are not perfectly parallel or by smoothing out the Fabry-Perot interference fringes by means of Fourier filtering. In case of weak absorption $\kappa \ll n$, the reflectivity is entirely determined by n and not suitable to derive κ by using a Kramers-Kronig transformation. At the same time, κ can be determined very accurately from the transmission. Since $T(\omega)$ depends exponentially on $\kappa \cdot d$, the appropriate choice of d is essential. Furthermore, the thickness d determines the effective “resolution” given by the interference fringes.

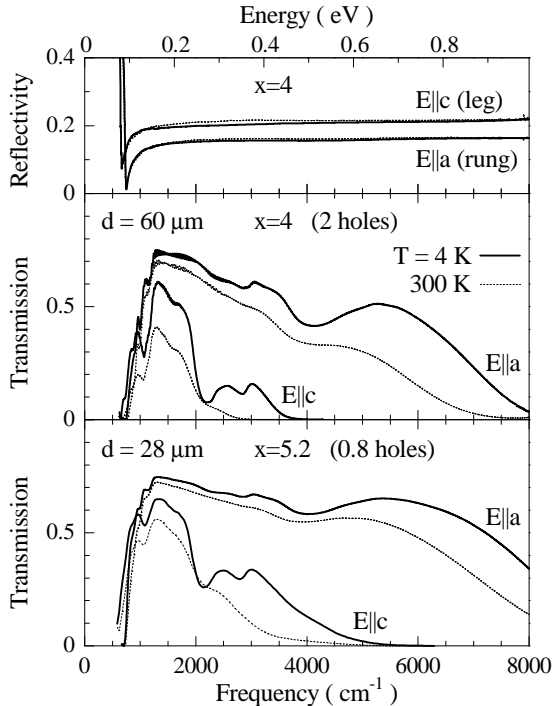


FIG. 1. Midinfrared reflectivity and transmission of $\text{La}_x\text{Ca}_{14-x}\text{Cu}_{24}\text{O}_{41}$ at 4 and 300 K.

The period of the fringes is given by $\Delta\tilde{\nu} = (2nd)^{-1}$, where $\Delta\tilde{\nu}$ is given in wave numbers if d is given in units of cm. Thus, a large value of d has the advantage of narrow fringes with a small amplitude, but strongly restricts the maximum value of κ that can be observed.

The top panel of Fig. 1 shows the reflectivity measured on a 0.8 mm thick sample ($x=4$) for polarization of the electrical field both parallel to the rungs and to the legs. At about 600-700 cm^{-1} one can observe the oxygen bond stretching phonon mode. At higher frequencies, the reflectivity is featureless, which is characteristic for the weak absorption regime below the gap of an insulator. We plotted the data for both 4 K (thick lines) and 300 K (thin dashed lines), but in $R(\omega)$ they are almost indistinguishable. The different absolute values of the two polarization directions reflect the difference in n , namely, $n_a \approx 2.3$ and $n_c \approx 2.6$. The weak absorption features we are looking for can only be detected in a transmission experiment, which also reveals a strong temperature dependence. The middle and bottom panels of Fig. 1 show $T(\omega)$ measured on thin single crystals with $x=4$ ($d=60\mu\text{m}$) and $x=5.2$ ($d=28\mu\text{m}$). The data in the middle panel were measured with a resolution of 4 cm^{-1} and show only small interference fringes, most probably because the sample surfaces were not perfectly parallel. The sample with $x=5.2$ (bottom panel) showed strong interference fringes with a period of $\approx 70 \text{ cm}^{-1}$, which have been removed by Fourier filtering.

In order to obtain a qualitative estimate of the absorption features it is common to approximate Eq. 2 by

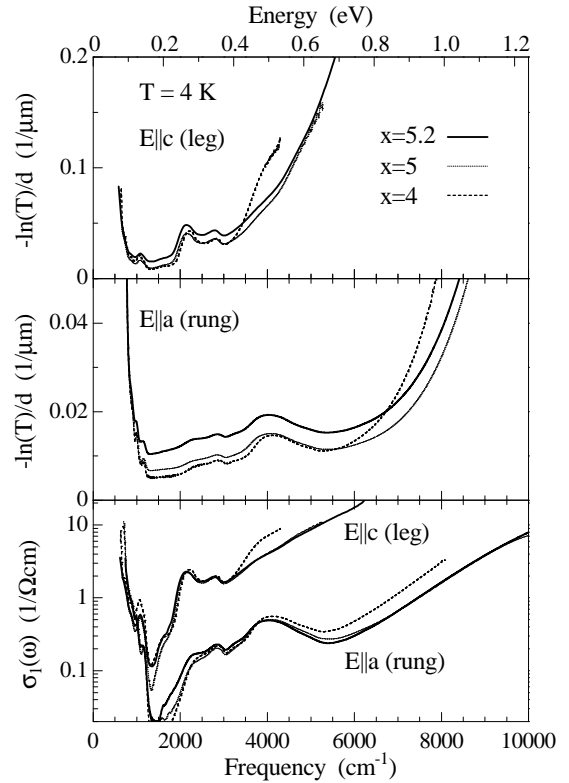


FIG. 2. Bottom panel: $\sigma_1(\omega)$ of $\text{La}_x\text{Ca}_{14-x}\text{Cu}_{24}\text{O}_{41}$ ($x=4, 5, \text{ and } 5.2$) at 4 K, calculated from transmission and reflectivity after Eq. 2. Top and middle panel: Plotting the logarithm of the transmission divided by the sample thickness already gives a qualitative estimate of the absorption features without knowledge of the reflectivity.

$$T(\omega) \approx (1 - R)^2 \Phi. \quad (4)$$

In this case one obtains the absorption coefficient $\alpha(\omega)$ as

$$\alpha(\omega) \approx -\ln(T)/d + 2\ln(1 - R)/d. \quad (5)$$

Neglecting the almost constant second term, we plot $-\ln(T(\omega))/d$ for $x=4, 5, \text{ and } 5.2$ at 4 K in the top ($E \parallel c$) and middle panels ($E \parallel a$) of Fig. 2. For comparison, the optical conductivity $\sigma(\omega)$ as derived by inverting Eq. 2 without further assumptions is displayed in the bottom panel of Fig. 2. In $\sigma(\omega)$ the curves for $x=5$ and $x=5.2$ almost fall on top of each other. Note that the erroneous discrepancy between these two data sets in $-\ln(T)/d$ is *not* due to a difference in $R(\omega)$, but due to the approximation used in Eq. 4. A precise and reliable determination of $\sigma(\omega)$ in the case of small absorption thus requires the measurement of *both* the transmission T and the reflectivity R and the use of Eq. 2.

III. Magnetic contribution to $\sigma(\omega)$

The spectra of $\sigma(\omega)$ can be divided into three different regimes. The absorption below $\approx 1300 \text{ cm}^{-1}$ can be attributed to phonons and multi-phonon bands. The strong

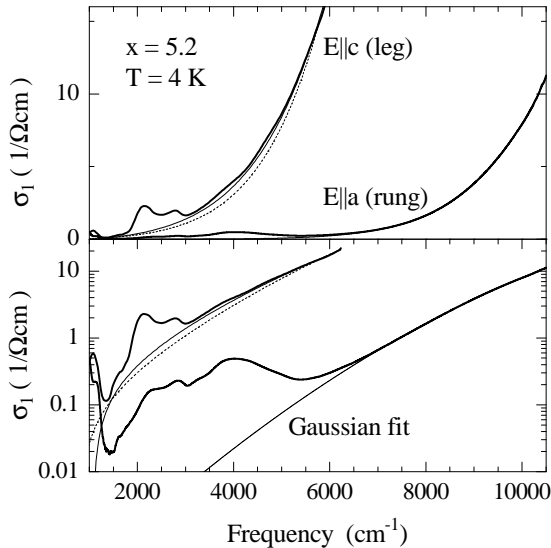


FIG. 3. Optical conductivity $\sigma_1(\omega)$ of $\text{La}_{5.2}\text{Ca}_{8.8}\text{Cu}_{24}\text{O}_{41}$ at 4 K (thick lines) on a linear (top panel) and on a logarithmic scale (bottom panel). The thin lines show Gaussian fits of the electronic background. For $E \parallel a$ the fit is unambiguous. For $E \parallel c$ two different background fits are shown in order to illustrate the uncertainty (see Fig. 4).

increase at high frequencies is due to an electronic background, which most probably has to be identified with the onset of charge-transfer excitations. We focus on the features in the intermediate frequency range. In order to analyze them we used Gaussian fits [15] to subtract the electronic background (thin lines in Fig. 3). For $E \parallel a$, the background can be determined unambiguously by fitting the measured data for $\omega > 7000 \text{ cm}^{-1}$. After subtraction of the background the $\sigma_a(\omega)$ curves are nearly independent of x , which corroborates the assumption that the ladders are undoped. For $E \parallel c$, the higher absorption complicates the determination of the background considerably. We were able to measure the transmission up to $\approx 6200 \text{ cm}^{-1}$ (in case of the $x=5.2$ sample with $d=28 \mu\text{m}$). Although this is a significant improvement compared to our earlier work [9] which was restricted to $\omega \lesssim 5000 \text{ cm}^{-1}$ ($x=5$), it is not yet sufficient for an unambiguous determination of the background. Therefore we show two different possibilities for Gaussian fits of the c -axis background in Fig. 3.

The estimates of the magnetic contribution to $\sigma(\omega)$ which we have obtained this way are plotted in Fig. 4 (thin and thick solid lines). In Ref. [9] we interpreted these features in terms of phonon-assisted two-triplet absorption [16], which was used to describe σ_1 of the undoped 2D cuprates (e.g. $\text{YBa}_2\text{Cu}_3\text{O}_6$ [17]) and of the 1D $S=1/2$ chain Sr_2CuO_3 [18]. Because of spin conservation two triplets are excited. The simultaneous excitation of a phonon provides the symmetry breaking necessary to bypass the selection rule and at the same time takes care of momentum conservation [9,16,17]. This

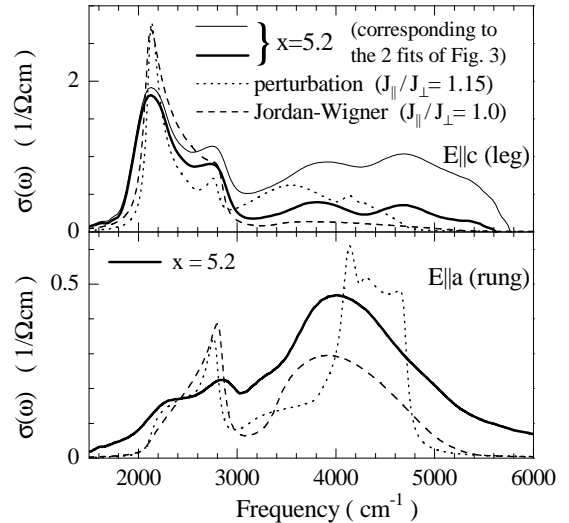


FIG. 4. Comparison of the magnetic contribution to the optical conductivity of $\text{La}_{5.2}\text{Ca}_{8.8}\text{Cu}_{24}\text{O}_{41}$ at 4 K (solid lines) and of the calculated results obtained with Jordan-Wigner fermions ($J_{\parallel}/J_{\perp} = 1.0$; $J_{\parallel} = 1100 \text{ cm}^{-1}$; dashed) and with optimized perturbation theory ($J_{\parallel}/J_{\perp} = 1.15$; $J_{\parallel} = 1080 \text{ cm}^{-1}$; dotted). In the top panel, the two different experimental curves (thin and thick solid lines) correspond to the two alternative background fits of Fig. 3.

process is the lowest order magnetic response possible in infrared absorption. The two peaks between 2000 and 3000 cm^{-1} (see Fig. 4) can be identified with the 1D van Hove singularities in the density of states of the strongly dispersing two-triplet bound state with $S_{\text{tot}}=0$ [9] (see below). The absorption at higher energies is attributed to the two-triplet continuum. The improved estimate of the background as compared to Ref. [9] allows us to detect *two* peaks within the continuum at about 3800 and 4700 cm^{-1} for $E \parallel c$. The precise determination of the spectral weight of these high energy features requires additional work. Note that also the a -axis spectrum displays a shoulder at high energies ($\approx 5000 \text{ cm}^{-1}$), although it is quite weak.

IV. Theory

Antiferromagnetic $S = 1/2$ two-leg Heisenberg ladders are represented by the Hamiltonian

$$\mathcal{H} = \sum_i \{ J_{\parallel} (\mathbf{S}_{1,i} \mathbf{S}_{1,i+1} + \mathbf{S}_{2,i} \mathbf{S}_{2,i+1}) + J_{\perp} \mathbf{S}_{1,i} \mathbf{S}_{2,i} \}, \quad (6)$$

where J_{\perp} and J_{\parallel} denote the rung and leg couplings, respectively. For $J_{\parallel}=0$ one can excite local rung singlets to rung triplets which become dispersive on finite J_{\parallel} (see Fig. 5). For $J_{\perp}=0$ the $S=1$ chain excitations decay into asymptotically free $S=1/2$ spinons. An intuitive picture of the “magnons” (elementary triplets) for $J_{\perp}, J_{\parallel} \neq 0$ can be obtained from both limits: the elementary excitations are either dressed triplet excitations or pairs of bound spinons with a finite gap Δ as long as $J_{\perp} > 0$ [10].

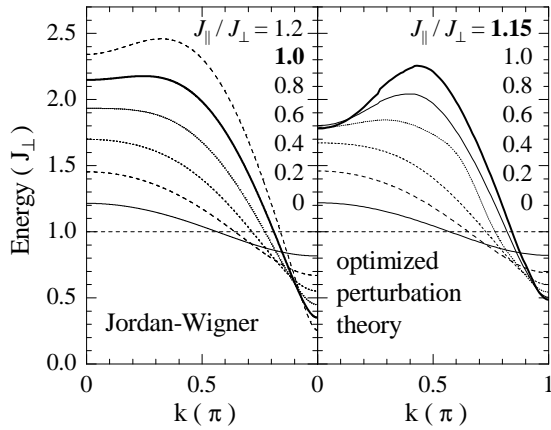


FIG. 5. Elementary triplet dispersion for $0 \leq J_{\parallel}/J_{\perp} \leq 1.2$. For each theory, the thick lines denote the coupling ratio that offers the best description of the optical conductivity of $(\text{La,Ca})_{14}\text{Cu}_{24}\text{O}_{41}$ (see Fig. 4).

Here, we present two theoretical approaches to describe the excitations of the ladder. One approach makes use of the Jordan-Wigner transformation to rewrite the spins as fermions with a long-ranged phase factor. Expanding the phase factor yields new interaction terms between the fermions. The resulting interacting fermion problem is treated diagrammatically. A similar treatment works very well for a 1D chain. The other approach uses an extrapolated perturbation in J_{\parallel}/J_{\perp} and separates contributions of different triplet number by continuous unitary transformations [8,10]. Both methods are controlled in the sense that they become exact on $J_{\parallel}/J_{\perp} \rightarrow 0$. In fact, comparing the results of these two methods for the dispersion of the elementary triplets (see Fig. 5), the agreement is excellent for $J_{\parallel}/J_{\perp} \leq 0.6$.

In order to determine the optical conductivity one needs to calculate the momentum-resolved two-particle spectral densities with $S_{\text{tot}} = 0$ [10]. The evolution of the spectral densities from $J_{\parallel}/J_{\perp} = 0.2$ to $J_{\parallel}/J_{\perp} = 1$ is plotted for both theories in Fig. 7. The optical conductivity as given in Fig. 6 is obtained by integrating these k -resolved curves with a weight factor $\omega \cdot \sin^4(k/2)$ [9]. For comparison with experiment one has to add the phonon energy as a constant shift of the energy scale (before multiplication by ω).

For $J_{\parallel}/J_{\perp} = 0.2$ the elementary triplet still shows only little dispersion (see Fig. 5). Therefore the two-particle continuum is rather narrow; the spectral weight is piled up at the bottom of the continuum for small momenta k , and for large k a bound state is formed below the continuum (see Fig. 7). For small ratios of J_{\parallel}/J_{\perp} this bound state reaches its maximum energy at the Brillouin zone boundary and dominates in $\sigma(\omega)$ as a single sharp peak with only a small continuum contribution at higher energies [5] (see left panels of Fig. 6). With increasing J_{\parallel}/J_{\perp} the bound state acquires a strong dispersion, and for $J_{\parallel}/J_{\perp} \gtrsim 0.5$ it shows a maximum at $k \approx \pi/2$ and

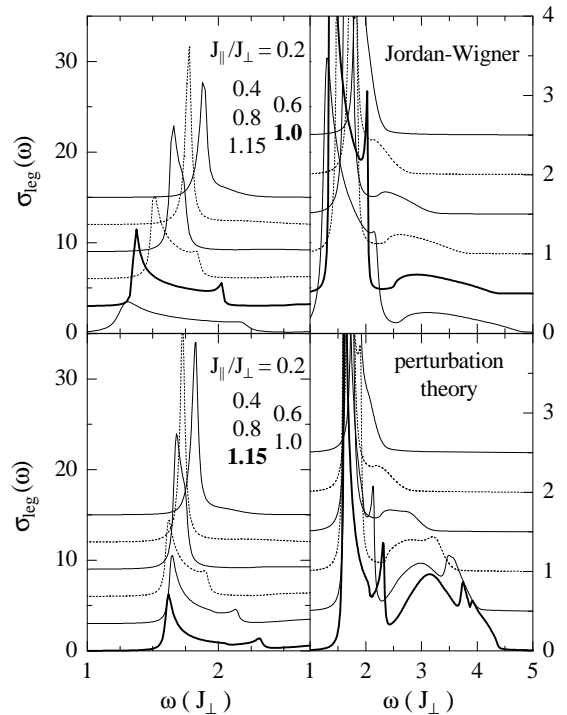


FIG. 6. Comparison of the optical conductivity for $E \parallel c$ (leg) calculated with Jordan-Wigner fermions (top panels) and with optimized perturbation theory (bottom) for $0 \leq J_{\parallel}/J_{\perp} \leq 1.15$. The left panels focus on the bound state, whereas the right panels emphasize the two-triplet continuum on an enlarged y -scale. For clarity, the curves were shifted with respect to each other by 3 (0.5) $(\Omega\text{cm})^{-1}$ in the left (right) panels. For each theory, the thick lines denote the coupling ratio that offers the best description of the bound states in $\sigma(\omega)$ of $(\text{La,Ca})_{14}\text{Cu}_{24}\text{O}_{41}$ (see Fig. 4). For comparison with experiment, the phonon frequency still has to be added (here: 600 cm^{-1}).

a minimum at the Brillouin zone boundary (see Fig. 7). Both give rise to van Hove singularities in the density of states which cause peaks in $\sigma(\omega)$. Therefore, the dominant peak observed for $J_{\parallel}/J_{\perp} = 0.2$ splits into two with increasing J_{\parallel} (see left panels of Fig. 6). Comparison of these spectra with the experimental data offers a very accurate tool to determine the exchange coupling constants, since the frequencies of the two peaks depend strongly on the coupling ratio J_{\parallel}/J_{\perp} [9]. For $\text{La}_{5.2}\text{Ca}_{8.8}\text{Cu}_{24}\text{O}_{41}$ we obtain $J_{\parallel}/J_{\perp} = 1.0$ and $J_{\parallel} = 1100 \text{ cm}^{-1}$ from the Jordan-Wigner fermions, whereas perturbation theory yields $J_{\parallel}/J_{\perp} = 1.15$ and $J_{\parallel} = 1080 \text{ cm}^{-1}$. This 15% discrepancy reflects the differences between the two theories that were already present in the dispersion of the elementary triplet (see Fig. 5). Both theories reproduce the experimental line shape rather well for both polarization directions. Note that the lower peak is suppressed for $E \parallel a$ due to symmetry [9].

A ratio of $J_{\parallel}/J_{\perp} \approx 1$ seems to be in conflict with several former results of other techniques, proposing $J_{\parallel}/J_{\perp} \gtrsim 1.5$ (see discussion in [19]). Such a rather small

value of J_{\perp} is suggested by the small spin gap observed in e.g. neutron scattering [20]. On the basis of our results we can exclude $J_{\parallel}/J_{\perp} > 1.2$ [9]. Recently, it was pointed out that the neutron data (i.e., the small spin gap) are also consistent with an isotropic exchange $J_{\parallel}/J_{\perp} \approx 1 - 1.1$ and $J_{\parallel} \approx 900 \text{ cm}^{-1}$, if a ring exchange of $J_{\text{cyc}} \approx 0.15 J_{\parallel}$ is taken into account [20]. Adding a finite ring exchange term reduces the gap at $k = \pi$ and washes out the dip in the triplet dispersion at small k [20,21]. Furthermore, the cyclic exchange weakens the attractive interaction between two rung triplets. We expect that these two changes, reduction of the dip and of the attractive interaction, render the theoretical predictions closer to the experimental findings of optical spectroscopy [21,22]. Since a $\approx 15\%$ ring exchange term is estimated [20,21] we expect a similar change in J_{\parallel}/J_{\perp} .

Finally, we address the evolution of the continuum with increasing J_{\parallel}/J_{\perp} (see Fig. 7). At small k , the spectral density is broadened strongly by the increase of the continuum width. Therefore, the $k=0$ Raman response shows a sharp peak for small J_{\parallel}/J_{\perp} and a broad band for $J_{\parallel}/J_{\perp} \approx 1$ (see Ref. [21] for more details). For large momenta one can observe the opposite, the features within the continuum become stronger and more pronounced with increasing J_{\parallel}/J_{\perp} . The mid-band line of square root singularities which runs from $k \approx \pi/2$ to $k = \pi$ denotes the upper edge of the precursor of the spinon continuum that is well known from the chain limit [10]. For $J_{\parallel}/J_{\perp}=1$ the perturbation result (top left panel of Fig. 7) shows additional pronounced features within the high energy part of the continuum [10]. The appearance of these features is related to the existence of the dip in the dispersion of the elementary triplet at small k (Fig. 5). Precursors of these features are present in perturbation theory for $J_{\parallel}/J_{\perp}=0.8$, where the dip in the dispersion is only small. The Jordan-Wigner fermions do not show these features.

In the weighted superpositions (Fig. 6) the perturbative results for $J_{\parallel}/J_{\perp} \geq 0.8$ display a second peak above $\omega \approx 3J_{\perp}$ in the high energy continua. The experimental data (Fig. 4) also display two peaks in the continuum, independent of the precise background correction. Yet the experimental peaks lie at higher energies and they are further apart from each other. On inclusion of ring exchange the calculated peaks will be shifted to higher energies since the attractive interaction is weakened. So we tentatively identify the two experimental with the two theoretical peaks even though their shape and mutual distance are not in perfect agreement. Further investigations including ring exchange are indispensable.

Summarizing, we reported in detail on one of the first observations of bound states in gapped spin systems. By phonon-assisted two-triplet absorption we were able to detect a bound state in the $S = 0$ channel resulting from two elementary triplets in the undoped spin ladder $\text{La}_x\text{Ca}_{14-x}\text{Cu}_{24}\text{O}_{41}$. The bound state exists for mo-

menta $k \gtrsim 0.3\pi$. Thus, it was decisive that phonons are involved in the optical excitation process in order to provide the necessary momentum. Two theoretical methods were employed to trace the evolution of the spectral densities as function of the coupling ratio J_{\parallel}/J_{\perp} . In both approaches the overall position and weight of the bound state agree well with the measurements. In experiment and in the perturbative approach two peaks in the continua are found. Some quantitative differences indicate that an extension of a simple spin ladder Hamiltonian is necessary. We argued that a 10-15% ring exchange term is the appropriate extension.

This project is supported by the DFG (FR 754/2-1, SP 1073 and SFB 484), by the BMBF (13N6918/1) and by the DAAD within the scope of PROCOPE.

-
- [1] M. Uehara *et al.*, J. Phys. Soc. Jpn. **65**, 2764 (1996).
 - [2] G.S. Uhrig and H.J. Schulz, Phys. Rev. B **54**, R9624 (1996); erratum *ibid.* **58**, 2900 (1998).
 - [3] K. Damle and S. Sachdev, Phys. Rev. B **57**, 8307 (1998).
 - [4] O.P. Sushkov and V.N. Kotov, Phys. Rev. Lett. **81**, 1941 (1998); V.N. Kotov, O.P. Sushkov, and R. Eder, Phys. Rev. B **59**, 6266 (1999).
 - [5] C. Jurecka and W. Brenig, Phys. Rev. B **61**, 14307 (2000).
 - [6] S. Trebst *et al.*, Phys. Rev. Lett. **85**, 4373 (2000).
 - [7] W. Zheng *et al.*, Phys. Rev. B **63**, 144410 (2001).
 - [8] C. Knetter and G.S. Uhrig, Eur. Phys. J. B **13**, 209 (2000).
 - [9] M. Windt *et al.*, Phys. Rev. Lett. **87**, 127002 (2001).
 - [10] C. Knetter, K.P. Schmidt, M. Grüninger, G.S. Uhrig, Phys. Rev. Lett. (2001), in press (cond-mat/0106077).
 - [11] U. Ammerahl and A. Revcolevschi, J. Crystal Growth **197**, 825 (1999); U. Ammerahl, PhD thesis, Univ. of Cologne, 2000.
 - [12] N. Nücker *et al.*, Phys. Rev. B **62**, 14384 (2000).
 - [13] M. Grüninger, Diplomarbeit, Univ. of Karlsruhe (1994).
 - [14] H.S. Choi, E.J. Choi, and Y.J. Kim, Physica C **304**, 66 (1998).
 - [15] In our earlier work [9], we subtracted an *exponential* background because the transmission was restricted to a narrower frequency range. The more recent data of Fig. 3 for $E \parallel a$ clearly show that a simple exponential fit is not sufficient. However, this has only a marginal effect on our estimate of the magnetic contribution to $\sigma(\omega)$. The only relevant difference is an improved description of the high energy continuum for $E \parallel c$.
 - [16] J. Lorenzana and G.A. Sawatzky, Phys. Rev. Lett. **74**, 1867 (1995); Phys. Rev. B **52**, 9576 (1995).
 - [17] M. Grüninger *et al.*, Phys. Rev. B **62**, 12422 (2000).
 - [18] H. Suzuura *et al.*, Phys. Rev. Lett. **76**, 2579 (1996); J. Lorenzana and R. Eder, Phys. Rev. B **55**, R3358 (1997).
 - [19] D.C. Johnston *et al.*, cond-mat/0001147.
 - [20] M. Matsuda *et al.*, Phys. Rev. B **62**, 8903 (2000); J. Appl. Phys. **87**, 6271 (2000).
 - [21] K.P. Schmidt, C. Knetter, and G.S. Uhrig, cond-mat/0107431.
 - [22] C. Knetter, K.P. Schmidt, and G.S. Uhrig, Physica B, in press (cond-mat/0107526).

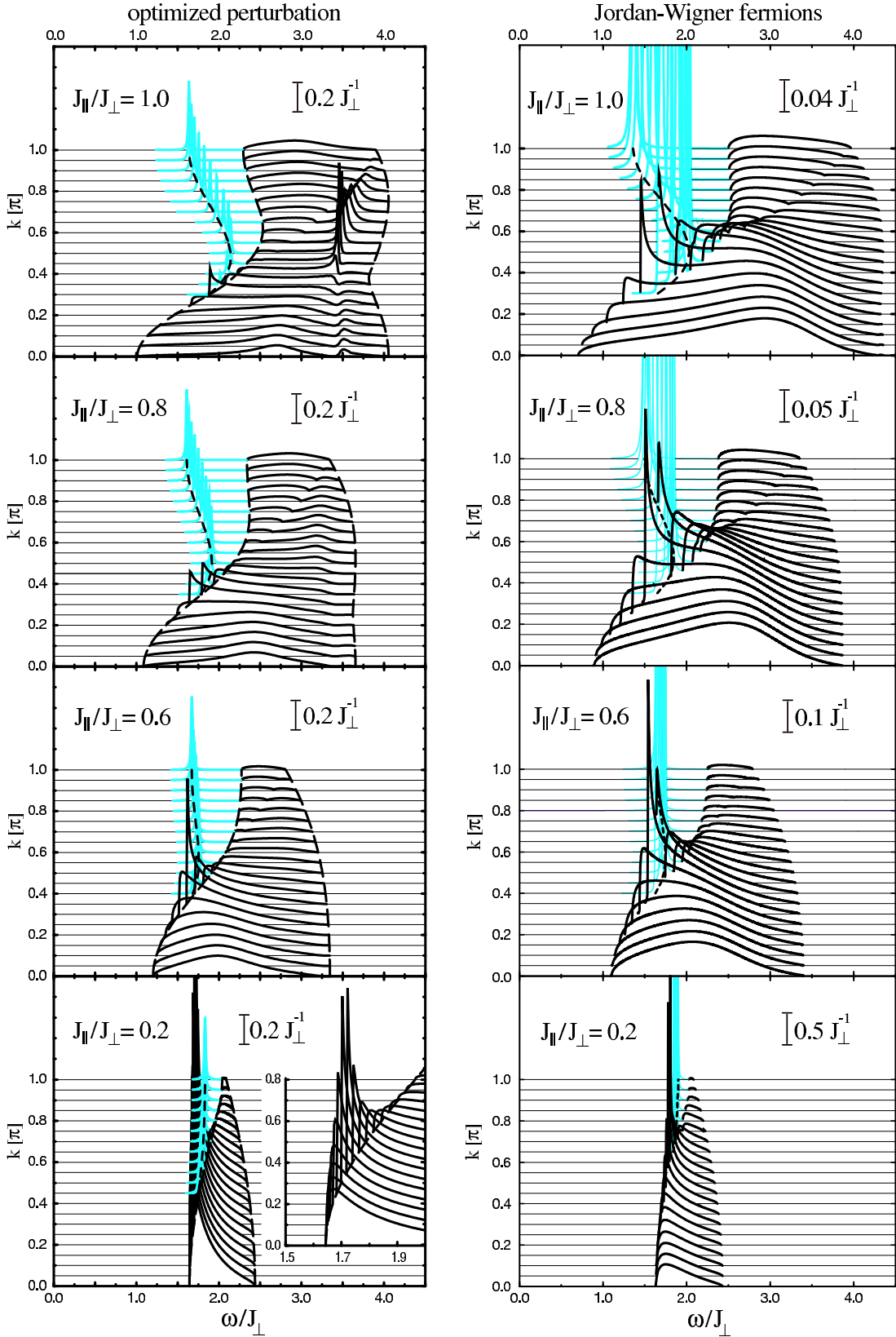


FIG. 7. Momentum dependence of the two-triplet spectral densities with $S_{tot} = 0$ for $E \parallel c$. Calculations were performed with optimized perturbation (left) and with Jordan-Wigner fermions (right) for $0 \leq J_{\parallel}/J_{\perp} \leq 1$. The k -resolved and ω -integrated weights for the two theories agree within 25% (note the different scalings of the plots). Gray curves represent the bound state, which was divided by 16 and artificially broadened by $J_{\perp}/100$ in the left panels. Black curves indicate the continuum. Inset of bottom left panel: enlarged view of the continuum, the bound state is not shown here.